ADVANCED MATERIALS
www.advmat.de

Injection of Microporous Annealing Particle (MAP) Hydrogels in the Stroke Cavity Reduces Gliosis and Inflammation and Promotes NPC Migration to the Lesion

*Lina R. Nih, Elias Sideris, S. Thomas Carmichael, and Tatiana Segura**

With the number of deaths due to stroke decreasing, more individuals are forced to live with crippling disability resulting from the stroke. To date, no therapeutics exist after the first 4.5 h after the stroke onset, aside from rest and physical therapy. Following stroke, a large influx of astrocytes and microglia releasing proinflammatory cytokines leads to dramatic inflammation and glial scar formation, affecting brain tissue's ability to repair itself. Pathological conditions, such as a stroke, trigger neural progenitor cells (NPCs) proliferation and migration toward the damaged site. However, these progenitors are often found far from the cavity or the peri-infarct tissue. Poststroke tissue remodeling results in a compartmentalized cavity that can directly accept a therapeutic material injection. Here, this paper shows that the injection of a porous hyaluronic acid hydrogel into the stroke cavity significantly reduces the inflammatory response following stroke while increasing peri-infarct vascularization compared to nonporous hydrogel controls and stroke only controls. In addition, it is shown that the injection of this material impacts NPCs proliferation and migration at the subventricular zone niche and results, for the first time, in NPC migration into the stroke site.

Stroke is the leading cause of long-term disability worldwide.[1] Ischemic stroke occurs when there is a decrease in cerebral blood flow due to an embolus or local thrombosis causing brain tissue damage and loss of function.[2] To date, intravenous thrombolysis and reperfusion therapies using intravenously administered recombinant tissue plasminogen activator (tPA) are the only effective therapies to treat stroke.[3] However, tPA is only effective during the first 4.5 h after stroke onset, resulting in only about 5% of stroke patients benefiting from this treatment and leaving the majority of patients with long term disability.[2,4] Besides physical therapy, there are no Food and Drug Administration approved therapies that promote recovery from the long-term disability caused by stroke, leaving an increasing number of patients with limited options.[5] Over the past few years, new strategies aimed at enhancing poststroke brain plasticity have utilized trophic factors, stem cell therapies or combinations of the two in an effort to decrease the disability burden.[6] One goal in these therapies is to promote neural progenitor cell (NPC) migration toward the stroke site in efforts to promote neurogenesis in and around the lesion. NPCs hold great promise for stroke repair because of their potential to generate all neural cell types present in the brain.[7] The stroke alone causes a substantial increase in NPC proliferation in the subventricular zone (SVZ);[8] however, these NPCs do not reach the stroke site itself in large numbers if it is distant to the SVZ.[9] Thus, approaches to further guide NPC migration toward the stroke site do so by delivering exogenous growth factors and cytokines to stimulate migration toward the stroke site, and differentiation into neurons.[10] Although improved NPC numbers in the peri-infarct area are observed, these NPCs are do not localize within the close damage to the stroke or into the stroke cavity.[9] Herein, we present a material that for the first time promotes the infiltration of endogenous NPCs from the SVZ into the stroke cavity.

Stroke offers a unique opportunity for a tissue engineering neural repair therapy. After initial cell death in stroke, the clearance of debris in the lesion leaves a compartmentalized cavity that can accept a large volume transplant without further damaging the surrounding healthy parenchyma.[11,12] This stroke cavity is situated directly adjacent to the peri-infarct tissue, the region of the brain that undergoes the most substantial repair and recovery, meaning that any therapeutic delivered to the cavity will have direct access to the tissue target for repair.[13] Our laboratory and others have investigated the use of injectable hydrogels injected poststroke to promote brain repair. These hydrogels are delivered to the mentioned stroke cavity, to the peri-infarct area or to the brain surface loaded with cells, trophic factors, and/or growth factors.[14] Hyaluronic acid (HA)

Dr. L. R. Nih, E. Sideris, Prof. T. Segura
Department of Chemical and Biomolecular Engineering
University of California
Los Angeles, 420 Westwood Plaza, CA 90095, USA
E-mail: tsegura@ucla.edu
Dr. L. R. Nih, Prof. S. T. Carmichael
Department of Neurology
David Geffen School of Medicine
University of California
Los Angeles, 621 Charles Young Drive, CA 90095, USA
Prof. T. Segura
Department of Dermatology
David Geffen School of Medicine
University of California
Los Angeles, 200 UCLA Medical Plaza, 90095, USA

DOI: 10.1002/adma.201606471

is an ideal choice to generate materials for brain repair. HA, unlike collagen, is abundantly found in the brain, particularly in the endogenous environment for NPCs[15] and is both a biocompatible and bioresorbable material.[16] We have previously reported the use of nonporous hyaluronic acid hydrogels crosslinked in situ via thiol/acrylamide Michael type addition for brain repair.[6,17,18] These materials demonstrated biocompatibility after transplantation in vivo when degradable soft materials were used, and the ability to promote vascular infiltration within the stroke cavity through delivery of vascular endothelial growth factor[18] or cells into the stroke cavity.[6,17] However, these approaches did not result in enhanced endogenous NPC migration to the stroke cavity. Similar approaches using hyaluronic acid hydrogels that sustain delivery of direct neurogenesis-inducing growth factors, such as brain-derived neurotrophic factor, does not induce neuroblast migration into the stroke cavity.[12]

Here, we demonstrate that injectable particle hydrogels—termed "microporous annealed particle" or MAP hydrogels—induce a tissue response that unlike nonporous materials leads to progenitor cell migration into the stroke cavity. In this material, hydrogel microspheres are annealed to each other to form a bulk scaffold and pore size is determined by the random packing of the microspheres. Like their nonporous counterpart, this MAP hydrogel has the benefit of being entirely injectable, which allows for a seamless boundary in addition to microporosity. Our particle hydrogel is injected as a μgel particle slurry directly to the stroke cavity, anneals in situ, and forms an interconnected porous scaffold that fills the entire cavity. This porous scaffold interacts with cells through integrin adhesion peptides and mediates rapid cellular infiltration through microporosity of the scaffold without the need for bulk scaffold degradation. Previously poly(ethylene glycol)-based particle hydrogels where shown to form mechanically stable scaffolds that enhanced cutaneous healing in vivo.[19] Here, HA MAP gels reduce brain inflammation post stroke, by promoting astrocyte infiltration into the stroke cavity rather than scar formation and reducing the total number of reactive microglia within the infarct. These events lead to an environment that allows neuroprogenitor cell migration into the material and stroke cavity.

HA MAP hydrogels were synthesized in three stages as previously described.[20] First, hyaluronic acid was modified through carbodiimide chemistry to introduce crosslinkable acrylamide groups (HA-Ac) on the HA backbone. Second, this polymer was modified with three peptides (adhesion peptide RGD and two Factor XIIIa substrates: Ac-FKGGERCG-NH_2, K-peptide, and Ac-NQEQVSPLGGERCG-NH_2, Q-peptide), and then crosslinked through Michael-type addition using a dicysteine-containing matrix metalloproteinase degradable peptide. The crosslinking takes place in an oil-coated aqueous droplet generated in a microfluidic device, resulting in highly monodisperse beads, or microgels (μgels), that will serve as MAP-gel building blocks (**Scheme 1**). These μgels were purified to remove oil and surfactants using repeated washing with buffer and centrifugation. Third, the μgels were linked to each other with factor XIIIa to form an annealed solid with void

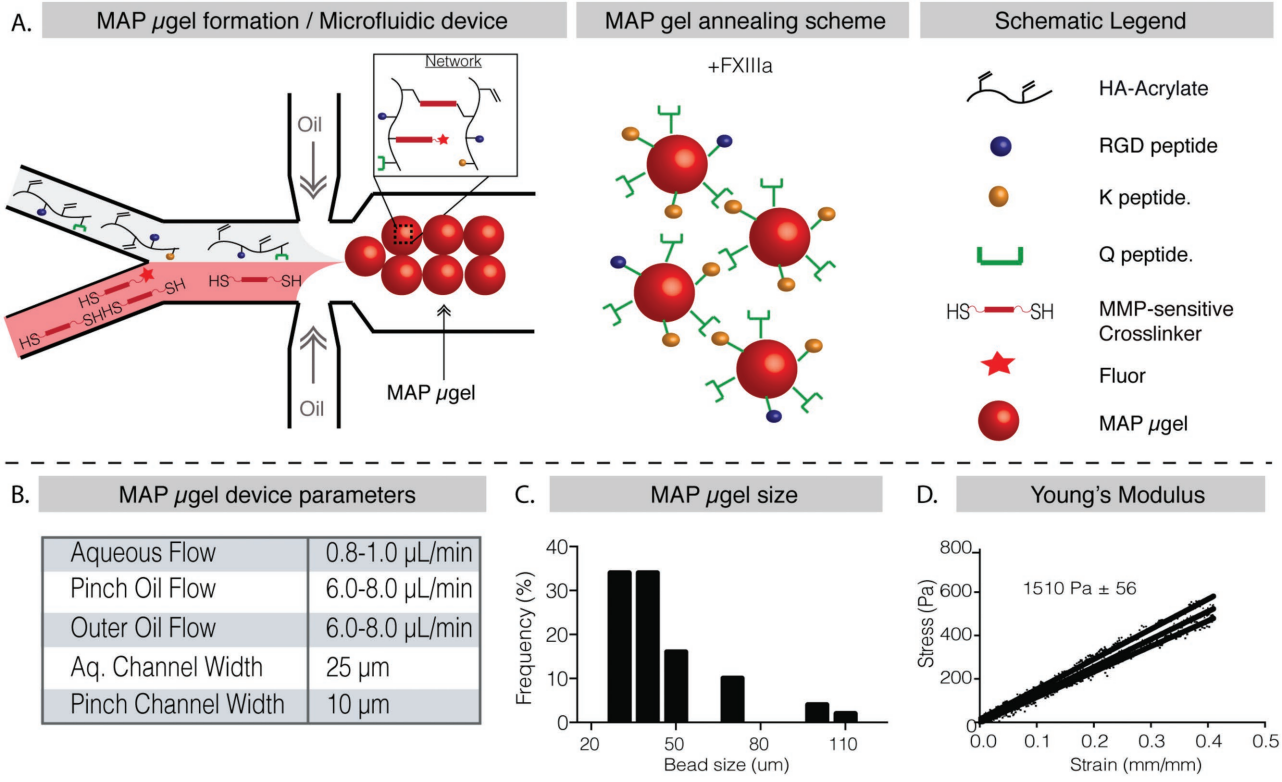

Scheme 1. A) Schematic illustration of flow focusing microfluidic device to produce μgels that can be annealed to each other using enzyme factor XIII to form a scaffold. B) Important flow rates and device parameters to produce the μgels. C) Distribution of μgels diameters produced using the microfluidic device. D) Young's modulus in compression calculated using Instron mechanical tests showing scaffold stiffness similar to brain cortex.

spaces (Figure S1, Supporting Information). The MAP hydrogel was labeled during μgel generation (step two described above) using a malemide-containing fluorophore such that the MAP scaffold can be imaged with standard confocal microscopy after sectioning (Scheme 1A).

The droplet microfluidic device is shown in (Scheme 1A). HA-Ac solution prereacted with the K, Q, and RGD peptides was flowed through one channel and matrix metalloproteinase (MMP) sensitive cross-linker was flowed in the second channel. These two channels merge to form the hydrogel precursor solution, which is quickly pinched by heavy mineral oil containing 1% surfactant to form μgels. The flow regime used (1 μL min^{-1} for the aqueous flow and 8 μL min^{-1} for the oil flow) produced a relatively narrow range of μgel sizes with an average μgel diameter of 45 μm (Scheme 1B,C). To determine the mechanical properties of annealed scaffolds purified μgels were mixed with activated FXIII (FXIIIa) and allowed to anneal for 90 min. Instron mechanical testing on the resulting annealed scaffold revealed a Young's modulus of 1510 Pa (Scheme 1D), which closely matches the stiffness of native cortex tissue of the brain.[17] Moreover, a concentrated solution of nonannealed microgels does not exhibit the mechanical properties of an annealed scaffold (Figure S1D, Supporting Information). Further, through atomic fluorescence microscopy of individual microgels and instron mechanical testing of annealed scaffold we have shown that the mechanical stiffness of individual microgels closely matches the mechanical stiffness of annealed scaffolds. Finally, we have previously conducted degradation studies and have shown that the microgels degrade in the presence of collagenase I.[20]

Our goal is to design HA MAP gels to promote brain tissue repair after stroke. Thus, we first studied the hydrogel injection and immune reaction toward HA MAP scaffolds to ensure that they will not further aggravate the brain damage after stroke. Brain ischemic strokes in the sensorimotor cortex were created using a middle cerebral artery occlusion (MCAo) model.[21] HA MAP or HA nanoporous hydrogels (6 μL) were injected into the cavity 5 d poststroke and animals were sacrificed 10 d postinjection. A group of mice with stroke but no gel injection (No Gel) was used as a negative control. MAP injection into the stroke cavity did not cause brain swelling or deformation and filled the entire cavity (**Figures 1**A and **2**A), indicating that the gel injection and hydrogel annealing in situ did not affect the brain structure. We next analyzed the inflammatory response to hydrogels by assessing astrogliosis (Figure 1B) and microgliosis (Figure 1C) 10 d postinjection. Astrogliosis was assessed through glial fibrillary acidic protein (GFAP) staining by measuring the astrocytic scar thickness and total percent positive signal in the infarct (within the stroke) and peri-infarct (around the stroke) regions. We observed a drastic decrease in the astrocytic scar thickness surrounding the MAP gel compared to the nanoporous (npore) gel and the No Gel condition (Figure 1D). The scar in the MAP condition was only 43 ± 8 μm thick while in the nanoporous gel and No Gel conditions, the scar was 234 ± 54 and 325 ± 69 μm thick, respectively, almost a 6x difference. This led to a lower percentage of astrocytes in the peri-infarct area of the MAP gel condition (Figure 1C). These results show that introducing a hydrogel decreases the scar thickness, while introducing microporosity in the hydrogel drastically reduces the scar thickness. However, analysis of the GFAP signal within the stroke cavity revealed a statistical increase for both the MAP condition and the nanoporous condition compared to the No Gel control (Figure 1D). This observation was surprising as we have not previously observed substantial GFAP positive cells infiltrating the stroke cavity. Further analysis showed that MAP gel injection promoted astrocyte infiltration into the infarct with an average infiltration length of 279 ± 71 μm compared to only 42 ± 19 μm in the nanoporous condition causing a higher percentage of astrocytes to occupy the infarct area in the MAP gel condition (Figure 1D). Interestingly these differences in astrocyte infiltration are due to the topography of the scaffold alone as the MAP and nanoporous scaffolds have the exact same biochemical signals and bulk moduli. To our knowledge this is the first time a porous hydrogel has been injected into the brain.

Similarly, significant differences in microglial response, assessed by the IBA-1 (ionized calcium binding adaptor molecule-1) signal were observed (Figure 1E). The percent area occupied by the microglia was significantly reduced in both the infarct and peri-infarct areas in the MAP gel condition compared to the nanoporous and No Gel conditions. While only 19% of the infarct area was positive for microglia in the MAP condition, 58% of the infarct area in the nanoporous condition, and 50% in the No Gel conditions were positive for IBA-1. Again the differences observed are solely due to the porosity of the gel and further support previous findings that the transplantation of porous materials in other tissues lead to a decrease in inflammatory cells in and around the scaffold implant site.[19,22] Taken together we show that both astrogliosis and microgliosis are significantly reduced in animals injected with MAP gels resulting in reduced scar thickness and decreased reactive microglia.

Once we had examined the inflammatory response, we observed cells within the infarct of the MAP condition that were not stained for astrocytes or microglia. Therefore, we wanted to determine the phenotype of those cells by investigating the vascular (Figure S2A, Supporting Information) and axonal infiltration (Figure S2B, Supporting Information) in both conditions. Based on our experience with MAP gels in skin[19] we expected to observe significant vascular ingrowth into the MAP scaffold but not in the nanoporous scaffold. However, we found very little vascular infiltration into the stroke/hydrogel region in all three conditions. Further analysis showed a significantly higher percentage of vessels in the peri-infarct area of the MAP gel (22%) compared to both nanoporous gel and No Gel conditions (6%) (Figure S2B, Supporting Information). These results highlight the fact that different tissues have substantially different postimplantation reactions to the same material. Brain tissue remodels slower than skin tissue and will likely require other bioactive signals beyond the scaffold for revascularization such as growth factors. The increase of vessels in the peri-infarct area for MAP over nanoporous is interesting because the material has no contact with this area. This implies that the modified inflammatory reaction in the MAP-treated animals lead to a proangiogenic peri-infarct environment. To assess axonal infiltration, we stained for the axonal marker NF200, which stains for the neurofilament cytoskeleton of axons and quantified the positive signal within the infarct area. We observed no

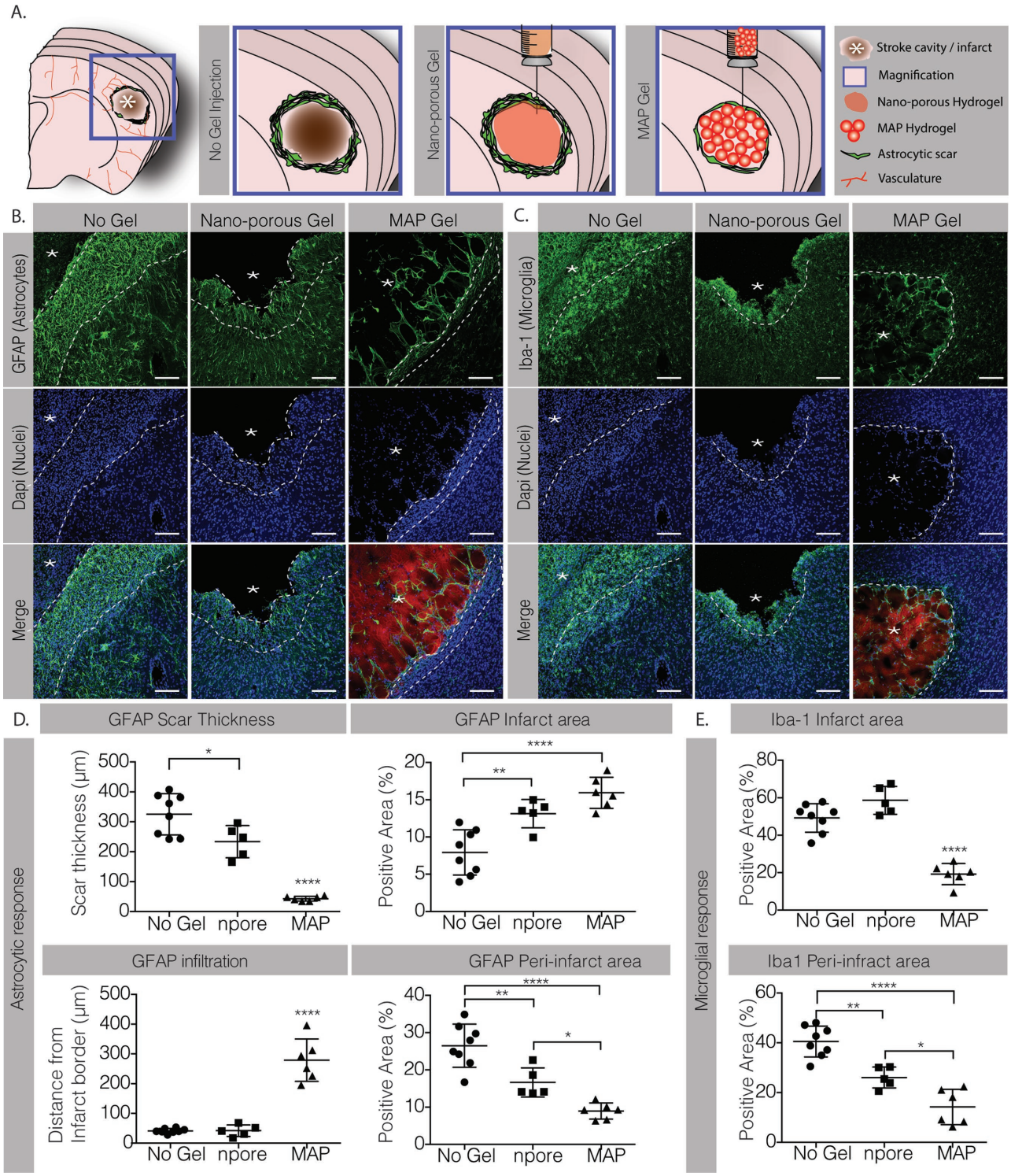

Figure 1. A) Schematic illustration of a coronal mouse brain section showing the location of the cortical stroke cavity. The magnified schematics illustrate the No Gel, the nanoporous, and the MAP hydrogel injection conditions. B) Fluorescent images of GFAP staining showing poststroke astrocytic response in the different conditions (scale bar: 100 µm). C) IBA-1 staining showing poststroke microglial response in the different conditions (scale bar: 100 µm). D) Analysis of the GFAP positive response in terms of scar thickness, astrocytic infiltration in the infarct area, and the positive area for GFAP signal in both infarct and peri-infarct regions. E) Analysis of the IBA-1 positive response in terms of positive area for GFAP signal in both infarct and peri-infarct regions. *, **, and **** indicate $P < 0.05$, $P < 0.01$, and $P < 0.0001$, respectively (Anova 1 way, Tukey's post hoc test).

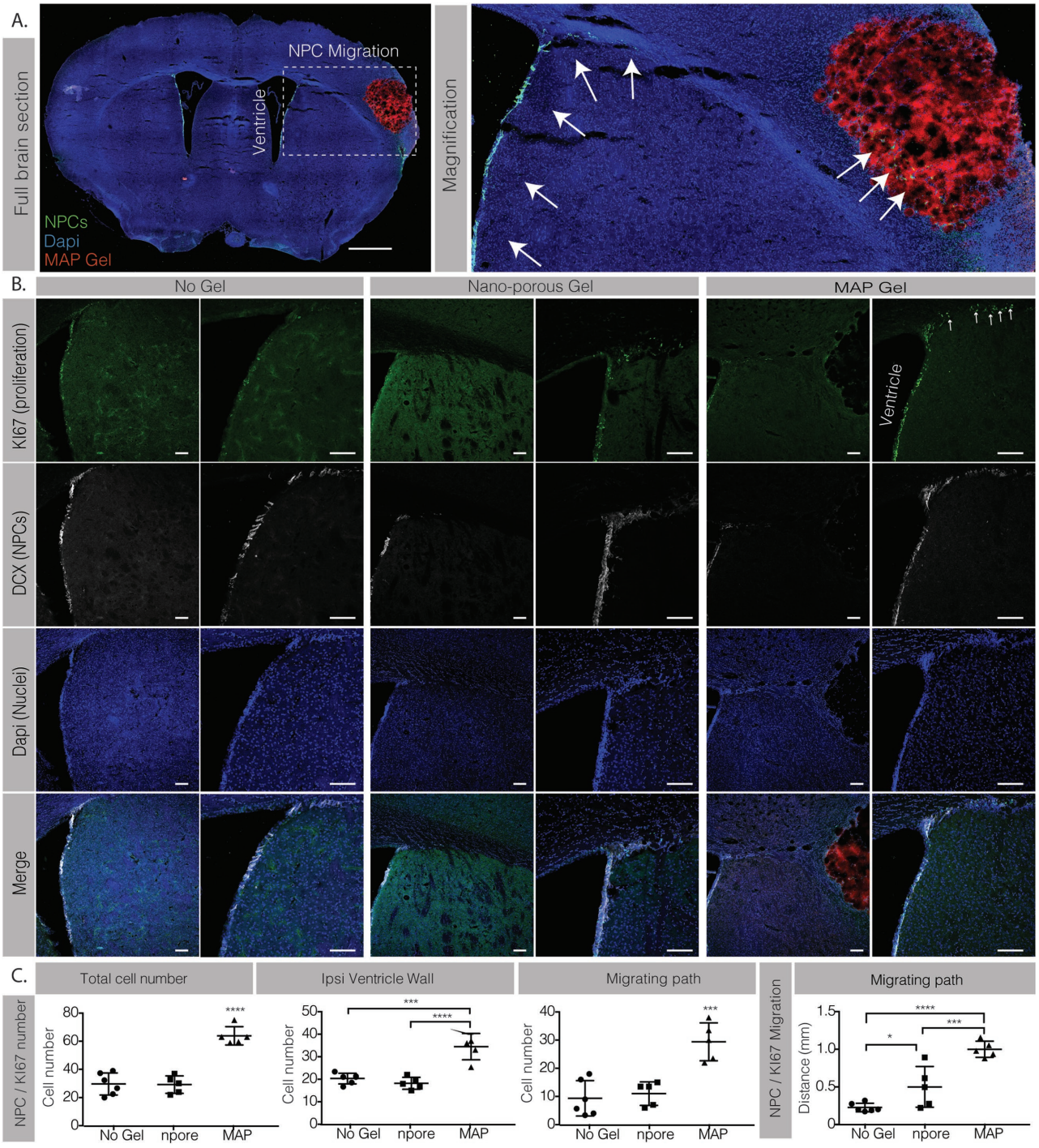

Figure 2. A) Full section fluorescent image and magnification showing DCX positively labeled NPCs (green) migrating from the ipsilateral ventricle to the stroke area (scale bar: 0.5 mm). B) Co-staining of Ki67 (green) and DCX positive NPCs (white) (scale bar: 100 µm). C) Analysis of KI67/DCX total cell number and migrating distance. *, ***, and **** indicate $P < 0.05$, $P < 0.001$, and $P < 0.0001$, respectively (Anova 1 way, Tukey's post hoc test).

differences in axonal processes into the stroke site (Figure S2D, Supporting Information).

Progenitor cell migration toward the damaged tissue is a poststroke spontaneous endogenous response that promotes tissue repair. However, due to inhibitory environmental cues at the injury site these progenitor cells do not always reach the diseased tissue nor lead to tissue repair.[9] In the brain, NPCs reside in the SVZ and the dentate gyrus and are activated after injury to proliferate, migrate, and differentiate toward the injured tissue.[23] Thus, we next investigated NPC activation and whether our material increased their proliferation and migration from the SVZ (Figure 2). To identify the NPCs

we stained for doublecortin (DCX) and for proliferating cells using Ki67. Cells that are double positive for DCX and Ki67 are considered proliferating NPCs (Figure 2A). Three separate analyses were performed to characterize NPC activation: the cell number along the ventricle wall, the migrating cell number, and the migration distance from the SVZ (Figure 2B). Upon injury the NPC population begins to divide to self-renew.[8] We found that for animals injected with MAP hydrogels there was an average of 34 ± 6 NPCs per section along the ventricle wall, while the nanoporous treated animals had a significantly lower average of 18 ± 3 NPCs, a number similar to the No Gel condition (Figure 2C). As expected, NPCs were observed migrating along the corpus callosum toward the infarct. Almost triple the amount of proliferating NPCs were counted migrating toward the damaged tissue in the MAP condition versus the nanoporous and No Gel condition. The analysis of the migration distance from the tip of the ventricle toward the leading edge of the migrating cells revealed that the NPCs in the MAP condition migrated an average of 1 mm compared to less than 0.5 mm in the nanoporous condition. No differences were observed in both the NPC cell number along the ventricle wall and the migrating cell number between the nanoporous and No Gel condition, however, in the No Gel condition, the NPCs migrated less than 0.23 mm, less than half of the nanoporous condition (Figure 2C).

We next examined the peri-infarct and infarct areas to determine if NPCs were able to reach the infarct site at 10 d postimplantation (**Figure 3**). To our surprise we observed NPCs not only in the peri-infarct area but also in the infarct area of the MAP hydrogel condition only (Figure 3A,B). Indeed, there was no migration of NPCs in both the nanoporous and the No Gel conditions. This is an interesting piece of data as migrating NPCs into a stroke cavity has never been observed before. The NPCs migrated as far as 300 µm into the MAP scaffold and occupied 3.75% ± 1.2 of the stroke surface (Figure 3C). Interestingly, the migration pattern and distance appeared to be similar to that observed for astrocytes. Co-staining for NPC and astrocytes showed that the NPCs colocalized with the infiltrating astrocytes, suggesting that astrocyte penetration is paving a path for NPC infiltration. More studies need to be performed to better understand how astrocytes are guiding NPC migration into the damaged site and whether the astrocyte and NPC infiltration happens simultaneously or in sequence.

In conclusion, we demonstrate that injectable particle hydrogels—MAP hydrogels—accelerate brain repair processes by altering poststroke astroglyosis and inflammation, changes that lead to enhanced vascularization at the peri-infarct cavity and neural progenitor cell migration within the damaged site. The present material contains hyaluronic acid, MMP, K, Q, and RGD peptides as bioactive signals. Although it is likely that during the FXIIIa enzyme mediated annealing process, endogenous proteins present in the stroke cavity are incorporated into the material via the same chemistry, we do not believe this is the reason for the observed differences in inflammatory response upon material injection because FXIIIa enzyme was also added to the HA non porous condition. Rather, we believe that the porosity of the scaffold allows for a cell infiltration into the MAP hydrogel independently of scaffold degradation. The nanoporous hydrogel contains the same bioactive components

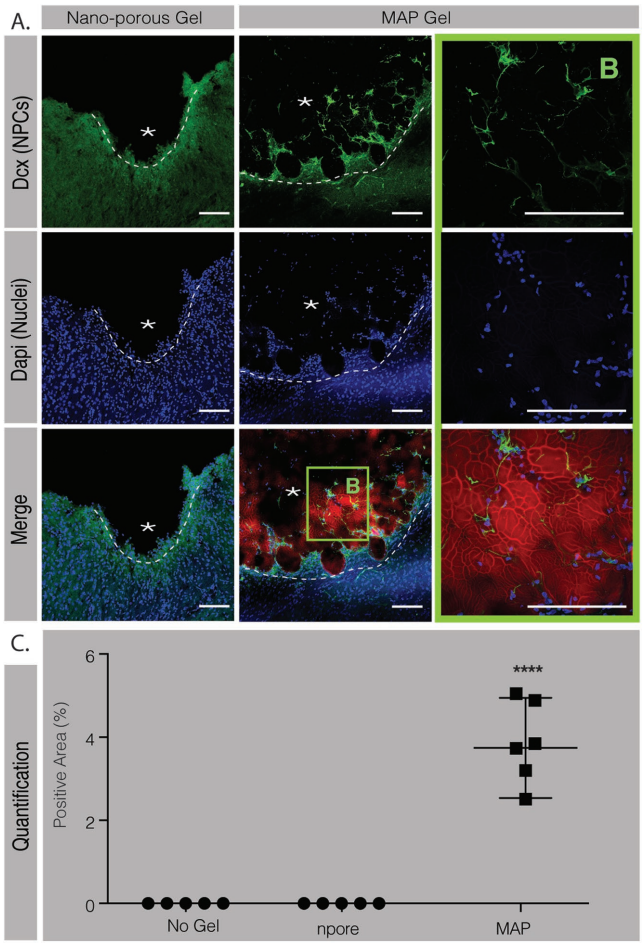

Figure 3. A) Fluorescent images and B) magnification of the stroke area in both the nanoporous and the MAP gel condition showing DCX positive cells (green) in the lesion site of the MAP–treated animals only (scale bar: 100 µm). C) Analysis of the positive area for DCX signal in the stroke site in the different conditions. **** indicates $P < 0.0001$ (Anova 1 way, Tukey's post hoc test).

and it did not result in reduced inflammatory reaction or NPC infiltration.

Experimental Section

Microgel Production and Purification: Microfluidic devices[19] and microgels[20] were produced as previously described. Briefly, an acrylate functionalized HA was dissolved at 7% (w/v) in 0.3 M triethyloamine (TEOA) pH 8.8 and prereacted with K-peptide (Ac-FKGGERCG-NH_2), Q-peptide (Ac-NQEQVSPLGGERCG-NH_2), and RGD (Ac-RGDSPGERCG-NH_2) at a final hydrogel concentration of 250, 250, and 500 µm, respectively. Meanwhile, the cross-linker solution was prepared by dissolving the di-thiol MMP sensitive linker peptide (Ac-GCRDGPQGIWGQDRCG-NH_2, Genscript) in distilled water at 7.8×10^{-3} M and reacted with 10×10^{-6} M Alexa-Fluor 488-maleimide (Life-Technologies) for 5 min. These solutions were mixed in a flow focusing microfluidic device and then immediately pinched by 1% span-80 in heavy mineral oil to form microspheres. These microspheres were collected and allowed to gel overnight to form microgels. The microgels were then purified by repeated washes with buffer and centrifugation. The swelling ratio of microgels has been previously

characterized when purified from the oil phase to the aqueous phase and found a 3.4× volumetric increase.[20]

Generation of Scaffold from Microgels and Mechanical Testing: The microgels were pelleted by centrifuging at 18 000 G and discarding the supernatant to form a concentrated solution of microgels. 5 U mL^{-1} of FXIII and 1 U mL^{-1} of Thrombin were combined in the presence of 10×10^{-3} M Ca^{2+} with the pelleted μgels and mixed via thorough pipetting before injection and allowed to incubate at 37 °C for 90 min between two slides (1 mm thickness) surface coated with sigmacote (Sigma-Aldrich). The mechanical testing on the hydrogel scaffolds was done using a 5500 series Instron. After annealing, the scaffolds were allowed to swell in HEPES buffer saline for 4 h at room temperature. A 2.5 N load cell with a 3.12 mm tip in diameter was used at a compression strain rate of 1 mm min^{-1} and the hydrogel scaffold was indented 0.8 mm or 80% of its total thickness.

Nanoporous Hydrogel Production: Nanoporous hydrogel precursor solutions were exactly the same as the microgel precursor solutions. As described in the *Microgel Production and Purification* section, an acrylate functionalized HA was dissolved at 7% (w/v) in 0.3 M TEOA pH 8.8 and prereacted with K-peptide (Ac-FKGGERCG-NH_2), Q-peptide (Ac-NQEQVSPLGGERCG-NH_2), and RGD (Ac-RGDSPGERCG-NH_2) at a final hydrogel concentration of 250, 250, and 500 μm, respectively. The molar ratio of acrylates to HA was 18.32, giving a concentration of 10.39×10^{-3} M of total acrylates. The total concentration of peptides was 1×10^{-3} M, giving a molar ratio 0.0962 moles of peptides per moles of acrylate. Finally, the molar ratio of thiols from cross-linker to moles of initial acrylates was 0.8, which gave a concentration of 8.31×10^{-3} M of thiols from cross-linker. The molar ratio of thiols from cross-linker to acrylates available after peptide conjugation was 0.88. The HA precursor solution was mixed with the peptides and allowed to react for 30 min before adding the cross-linker, FXIII, and thrombin. Using the precursor solution with the same concentration of peptides as the precursor solution to the microgels ensures that the concentration of peptides in the nanoporous hydrogel is the same as in the microgels. Moreover, the same cross-linker solution was prepared by dissolving the di-thiol MMP sensitive linker peptide in distilled water at 7.8×10^{-3} M and reacted with 10×10^{-6} M Alexa-Fluor 647-maleimide for 5 min. These two solutions were thoroughly mixed in an Eppendorf tube by vortexing and pipetting. 5 U mL^{-1} of FXIII and 1 U mL^{-1} of thrombin were added to the solution and the nanoporous hydrogel was allowed to gel in situ via the same Michael type addition in which the microgels were individually formed. The purpose of the addition of FXIII and thrombin was to mimic the microgel injections and to ensure that any phenomenon which was observed was not because of the added enzymes. Furthermore, scanning electron microscopy has been previously used to visualize the mesh size of these HA nanoporous hydrogels.[24]

Animal Stroke Model and Immunohistological Staining: Animal procedures were performed in accordance with the US National Institutes of Health Animal Protection Guidelines and the University of California Los Angeles Chancellor's Animal Research Committee. The mouse model of stroke was performed as previously described.[25] Briefly, a permanent cortical stroke was induced by a MCAo on young adult C57BL/6 male mice (8–12 weeks) obtained from Jackson laboratories. Briefly, under anesthesia, a small craniotomy was made over the left parietal cortex where an anterior branch of the distal middle cerebral artery was then exposed, electrocoagulated, cut to be permanently occluded, and bilateral jugular veins were clamped for 15 min. 5 d following stroke surgery, microgels with FXIIIa were loaded into a Hamilton syringe (Hamilton Reno, NV) connected to a pump and 6 μL of microgels were injected into the stroke cavity using a 30 gauge needle at stereotaxic coordinates 0.26 mm anterior/posterior (AP), 3 mm medial/lateral (ML), and 1 mm dorsal/ventral (DV) with an infusion speed of 1 μL min^{-1}. The needle was withdrawn from the mouse brain 5 min after the injection to allow for microgel annealing. Before injection, microgels were kept on ice to ensure that very little to no annealing would take place in the syringe during injection and all the annealing would occur in situ since FXIIIa has its highest activity at 37 °C. This was done to maintain consistency between the nanoporous and MAP conditions since it has been the shown that the mode of implantation plays a drastic role in the tissue response.[26] Preliminary observations showed that withdrawing the needle from the brain immediately after MAP gel injection was associated with a rapid and instant backflow of the gel, suggesting that the injected gel had not annealed by the end of the injection time (Video S1, Supporting Information). However, leaving the needle in place for 5 min after gel injection was not associated with any backflow, suggesting that the injected gel had begun annealing and forming a scaffold in the stroke cavity. For the nanoporous condition, 6 μL of hydrogel precursor solution (HA-acrylate + peptides + MMP sensitive cross-linker) with FXIIIa were injected into the stroke cavity using a 30 gauge needle at stereotaxic coordinates 0.26 mm AP, 3 mm ML, and 1 mm DV with an infusion speed of 1 μL min^{-1}. 10 d following the hydrogel transplantation, mice were sacrificed via transcardial perfusion of 0.1 M PBS followed by 40 mL of 4 (w/v)% paraformaldehyde (PFA). The brains were isolated and postfixed in 4% PFA overnight and submerged in 30 (w/v) % sucrose solution for 24 h. Tangential cortical sections of 30 μm thickness were sliced using a cryostat and directly mounted on gelatin-subbed glass slides for immunohistological staining of GFAP (Abcam, Cambridge, MA, USA) for astrocytes, IBA-1 (ionized calcium binding adaptor molecule, Abcam, Cambridge, MA, USA) for microglial cells, Glut-1 (Glucose Transporter-1, Abcam, Cambridge, MA, USA) for endothelial cells, NF200 (Neurofilament 200, Abcam, Cambridge, MA, USA) for axonal processes, DCX (Abcam, Cambridge, MA, USA) for NPCs, Ki67 (Abcam, Cambridge, MA, USA) for proliferating cells, and 4′,6-diamidino-2-phenylindole (DAPI) (1:500 Invitrogen) for nuclei. Primary antibodies (1:100) were incubated overnight at 4 °C and secondary antibodies (1:1000) were incubated at room temperature for 2 h. A Nikon C2 confocal microscope was used to take fluorescent images.

Image Analysis: Analyses were performed on microscope images of three coronal brain levels at +0.80, −0.80, and −1.20 mm according to bregma, which consistently contained the cortical infarct area. Each image represents a maximum intensity projection of 10 to 12 Z-stacks, 1 μm apart, captured at a 20× magnification with a Nikon C2 confocal microscope using the NIS Element software.

The endothelial (Glut-1), astrocytic (GFAP), and inflammation (IBA-1) positive area in the infarct and peri-infarct areas were quantified in 4 to 8 randomly chosen regions of interest (ROI of 0.3 mm^2). In each ROI, the positive area was measured using pixel threshold on 8-bit converted images using ImageJ (Image J v1.43, Bethesda, MD, USA) and expressed as the area fraction of positive signal per ROI (%). Values were then averaged across all ROI and sections, and expressed as the average positive area per animal.

The thickness of scar was measured on the ischemic boundary zone within the ipsilateral hemisphere on three sections stained for GFAP. The proliferating NPC cell count and migrating distance were measured on the ipsilateral hemisphere and represents the total number of doubele labeled DCX/Ki67 positive cells present on the ventricle wall and migrating toward the infarcted zone, the maximum migration distance of NPCs was measured between the upper corner of the ipsilateral wall on the corpus callosum and the furthest DCX/Ki67 positive cell on the migrating path toward the stroke site.

Supporting Information

Supporting Information is available from the Wiley Online Library or from the author.

Acknowledgements

L.R.N. and E.S. contributed equally to this work. This work was supported by the National Institutes of Health RO1NS094599 (TS) and R01NS081055 (STC). We would like to thank Prof. Donald Griffin and Dr. Sasha Cai Lesher-Perez for insight in microgel preparation.

Conflict of Interest

The authors declare that TS is a founder in Tempo Terapeutics, which seeks to commercialize MAP hydrogels.

Keywords

inflammation, neural progenitor cells, particle hydrogels, porous hydrogels, stroke

Received: November 29, 2016
Revised: March 27, 2017
Published online:

[1] A. S. Go, D. Mozaffarian, V. L. Roger, E. J. Benjamin, J. D. Berry, M. J. Blaha, S. Dai, E. S. Ford, C. S. Fox, S. Franco, H. J. Fullerton, C. Gillespie, S. M. Hailpern, J. A. Heit, V. J. Howard, M. D. Huffman, S. E. Judd, B. M. Kissela, S. J. Kittner, D. T. Lackland, J. H. Lichtman, L. D. Lisabeth, R. H. Mackey, D. J. Magid, G. M. Marcus, A. Marelli, D. B. Matchar, D. K. McGuire, E. R. Mohler 3rd, C. S. Moy, M. E. Mussolino, R. W. Neumar, G. Nichol, D. K. Pandey, N. P. Paynter, M. J. Reeves, P. D. Sorlie, J. Stein, A. Towfighi, T. N. Turan, S. S. Virani, N. D. Wong, D. Woo, M. B. Turner, *Circulation* **2014**, *129*, e28.

[2] P. Dibajnia, C. M. Morshead, *Acta Pharmacol. Sin.* **2013**, *34*, 78.

[3] G. A. Donnan, M. Fisher, M. Macleod, S. M. Davis, *Lancet* **2008**, *371*, 1612.

[4] J. T. Kim, G. C. Fonarow, E. E. Smith, M. J. Reeves, D. D. Navalkele, J. C. Grotta, M. V. Grau-Sepulveda, A. F. Hernandez, E. D. Peterson, L. H. Schwamm, J. L. Saver, *Circulation* **2017**, *135*, 2, 128.

[5] a) T. N. Taylor, P. H. Davis, J. C. Torner, J. Holmes, J. W. Meyer, M. F. Jacobson, *Stroke* **1996**, *27*, 1459; b) J. P. Broderick, *Stroke* **2004**, *35*, 205.

[6] P. Moshayedi, L. R. Nih, I. L. Llorente, A. R. Berg, J. Cinkornpumin, W. E. Lowry, T. Segura, S. T. Carmichael, *Biomaterials* **2016**, *105*, 145.

[7] a) B. A. Reynolds, S. Weiss, *Science* **1992**, *255*, 1707; b) B. A. Reynolds, S. Weiss, *Dev. Biol.* **1996**, *175*, 1.

[8] a) R. Zhang, Z. Zhang, L. Wang, Y. Wang, A. Gousev, L. Zhang, K. L. Ho, C. Morshead, M. Chopp, *J. Cereb. Blood Flow Metab.* **2004**, *24*, 441; b) R. L. Zhang, Y. LeTourneau, S. R. Gregg, Y. Wang, Y. Toh, A. M. Robin, Z. G. Zhang, M. Chopp, *J. Neurosci.* **2007**, *27*, 3157.

[9] O. Lindvall, Z. Kokaia, *CSH Perspect. Biol.* **2015**, *7*, a019034.

[10] a) J. Ohab, S. Fleming, A. Blesch, S. T. Carmichael, *J. Neurosci.* **2006**, *26*, 13007; b) P. Dadwal, N. Mahmud, L. Sinai, A. Azimi, M. Fatt, F. E. Wondisford, F. D. Miller, C. M. Morshead, *Stem Cell Rep.* **2015**, *5*, 166.

[11] D. Michalski, W. Hartig, M. Krueger, C. Hobohm, J. A. Kas, T. Fuhs, *Neuroreport* **2015**, *26*, 583.

[12] D. J. Cook, C. Nguyen, H. N. Chun, L. L. I, A. S. Chiu, M. Machnicki, T. I. Zarembinski, S. T. Carmichael, *J. Cereb. Blood Flow Metab.* **2016**, *37*, 1030.

[13] S. T. Carmichael, *Ann. Neurol.* **2016**, *79*, 895.

[14] a) A. Tuladhar, C. M. Morshead, M. S. Shoichet, *J. Controlled Release* **2015**, *215*, 1; b) M. Bacigaluppi, G. L. Russo, L. Peruzzotti-Jametti, S. Rossi, S. Sandrone, E. Butti, R. De Ceglia, A. Bergamaschi, C. Motta, M. Gallizioli, *J. Neurosci.* **2016**, *36*, 10529.

[15] P. Moshayedi, S. T. Carmichael, *Biomatter* **2013**, *3*, e23863.

[16] J. R. Fraser, T. C. Laurent, H. Pertoft, E. Baxter, *Biochem. J.* **1981**, *200*, 415.

[17] J. Lam, W. E. Lowry, S. T. Carmichael, T. Segura, *Adv. Funct. Mater.* **2014**, *24*, 7053.

[18] S. Zhu, L. Nih, S. T. Carmichael, Y. Lu, T. Segura, *Adv. Mater.* **2015**, *27*, 3620.

[19] D. R. Griffin, W. M. Weaver, P. O. Scumpia, D. Di Carlo, T. Segura, *Nat. Mater.* **2015**, *14*, 737.

[20] E. Sideris, D. R. Griffin, Y. Ding, S. Li, W. M. Weaver, D. Di Carlo, T. Hsiai, T. Segura, *ACS Biomater. Sci. Eng.* **2016**, *2*, 2034.

[21] S. T. Carmichael, *NeuroRx* **2005**, *2*, 396.

[22] a) L. R. Madden, D. J. Mortisen, E. M. Sussman, S. K. Dupras, J. A. Fugate, J. L. Cuy, K. D. Hauch, M. A. Laflamme, C. E. Murry, B. D. Ratner, *Proc. Natl. Acad. Sci. USA* **2010**, *107*, 15211; b) S. Sokic, M. Christenson, J. Larson, G. Papavasiliou, *Macromol. Biosci.* **2014**, *14*, 731; c) A. N. Stachowiak, A. Bershteyn, E. Tzatzalos, D. J. Irvine, *Adv. Mater.* **2005**, *17*, 399.

[23] D. Inta, H. A. Cameron, P. Gass, *Trends Neurosci.* **2015**, *38*, 517.

[24] T. Tokatlian, C. Cam, S. N. Siegman, Y. Lei, T. Segura, *Acta Biomater.* **2012**, *8*, 3921.

[25] L. R. Nih, N. Deroide, C. Lere-Dean, D. Lerouet, M. Soustrat, B. I. Levy, J. S. Silvestre, T. Merkulova-Rainon, M. Pocard, I. Margaill, N. Kubis, *Eur. J. Neurosci.* **2012**, *35*, 1208.

[26] A. Berdichevski, H. Simaan Yameen, H. Dafni, M. Neeman, D. Seliktar, *Proc. Natl. Acad. Sci. USA* **2015**, *112*, 5147.